LA-UR- 11-03191

Approved for public release; distribution is unlimited.

Title: Effect of an electric field on superfluid helium scintillation produced by alpha-particle sources

Author(s): Takeyasu Ito, Steven Clayton, John Ramsey, M. Karcz, C.-Y. Liu, J. C. Long, H.-O. Meyer, T.G Reddy, and G. Seidel

Intended for: Physical Review A

Los Alamos
NATIONAL LABORATORY
EST. 1943

Los Alamos National Laboratory, an affirmative action/equal opportunity employer, is operated by the Los Alamos National Security, LLC for the National Nuclear Security Administration of the U.S. Department of Energy under contract DE-AC52-06NA25396. By acceptance of this article, the publisher recognizes that the U.S. Government retains a nonexclusive, royalty-free license to publish or reproduce the published form of this contribution, or to allow others to do so, for U.S. Government purposes. Los Alamos National Laboratory requests that the publisher identify this article as work performed under the auspices of the U.S. Department of Energy. Los Alamos National Laboratory strongly supports academic freedom and a researcher's right to publish; as an institution, however, the Laboratory does not endorse the viewpoint of a publication or guarantee its technical correctness.

Form 836 (7/06)

LA-UR xx-xxxx; Draft Version 6.0 May 30, 2011

Effect of an electric field on superfluid helium scintillation produced by α-particle sources

T. M. Ito,* S. M. Clayton, and J. Ramsey
Physics Division, Los Alamos National Laboratory, Los Alamos, NM 87545

M. Karcz, C.-Y. Liu, J. C. Long, H.-O. Meyer, and T. G. Reddy
Department of Physics Indiana University, Bloomington, IN 47405

G. M. Seidel
Department of Physics, Brown University, Providence, RI, 02912
(Dated: May 31, 2011)

We report a study of the intensity and its time dependence of scintillation produced by weak α-particle sources in superfluid helium in the presence of an electric field ($0 - 45$ kV/cm) in the temperature range of 0.2 K to 1.1 K at the saturated vapor pressure. Both the prompt and the delayed components of the scintillation exhibit a reduction in intensity with the application of an electric field. The reduction in the intensity of the prompt component is well approximated by a linear dependence on the electric field strength with a reduction of 15% at 45 kV/cm. When analyzed using the Kramers theory of columnar recombination, this field dependence leads to the conclusion that 40% of the scintillation results species formed from atoms originally promoted to excited states and 60% from excimers created by ionization and subsequent recombination, with the charges initially having a cylindrical Gaussian distribution about the α track of 60 nm. The intensity of the delayed component of the scintillation has a stronger dependence on the electric field strength and on temperature. The implications of these data on the mechanisms in liquid helium affecting scintillation are discussed.

PACS numbers: 34.50.Gb, 33.50.-j,82.20.Pm

I. INTRODUCTION

The phenomenon of liquid helium (LHe) scintillation due to passage of charged particles was discovered in the late 1950's [1, 2]. Since then rather extensive studies have been conducted, motivated both by its intrinsic interest (including an interest in illuminating the behavior of ions and neutrals in superfluid helium) and by the application of liquid helium as a particle detector [3, 4]. (For a brief review of early work, see Ref. [5]. A more recent review can be found in the introduction of Ref. [4].)

The following picture has emerged from these studies as the process for liquid helium scintillation production (see e.g. Refs. [4, 7–9]): when a charged particle passes through liquid helium, it deposits energy to the medium, part of which goes to ionization, creating electron-ion pairs along its track. Atoms in excited states are produced as well. The W value, the average energy required to produce one electron-ion pair, in liquid helium is $W \sim 43$ eV [10]. Electrons and ions then thermalize with the liquid helium. The electron subsequently forms a "bubble" in the liquid, pushing away surrounding helium atoms as a consequence of Pauli exclusion. The He^+ ion, on the other hand, forms a "helium snow ball" attracting surrounding helium atoms. The bubbles and snow balls then recombine quickly ($\sim 10^{-11}$ s) forming excited helium molecules (excimers). The molecules are formed in the triplet and singlet states. The singlet state molecule, $He_2(A^1\Sigma_u^+)$, radiatively decays in less than 10^{-8} s to the (unbound) ground state, emitting a $\sim$ 16 eV ultraviolet photon, contributing to the prompt component of scintillation. Excited atoms in singlet states also contribute to the prompt scintillation signal. The triplet state molecule, $He_2(a^3\Sigma_u^+)$, on the other hand, has a lifetime life of $\sim$ 13 s in liquid helium [11, 12]. In a high excitation density environment, however, the triplet state excimers can also be destroyed through the Penning ionization process

$$He_2 + He_2 \rightarrow 3He + He^+ + e^-, \quad (1)$$

or

$$He_2 + He_2 \rightarrow 2He + 2He^+ + e^-. \quad (2)$$

If a singlet excimer is formed as a result of Penning ionization, it makes a contribution to the delayed scintillation component.

The study of liquid helium scintillation has been conducted mostly using radioactive sources, such as β, conversion electron, and α sources. Various characteristics of the scintillation light depend on the type of ionizing particles employed. When a β or conversion electron source is used, the scintillation light yield is known not to show a strong temperature dependence, whereas when the scintillation is induced by α particles, the scintillation yield does exhibit a temperature dependence. In addition, a

*Corresponding author. Electronic address: ito@lanl.gov

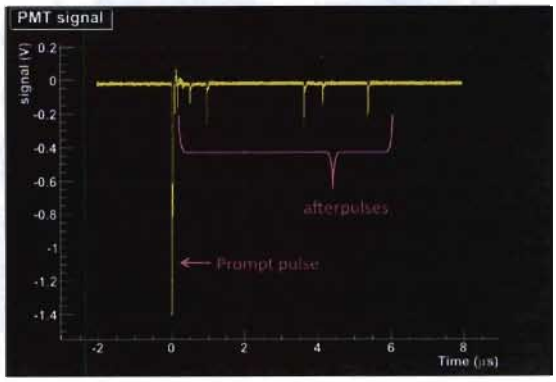

FIG. 1: Oscilloscope trace of a PMT signal of a typical signal

difference in time dependence of the scintillation signal has been observed between α-induced scintillation and β-induced scintillation [4]: α-induced scintillation light shows a long lived component that decays with a $1/t$ dependence following the prompt pulse . This slow component shows up as a series of single photoelectron (P.E.) pulses following the prompt pulse in an experiment in which the UV scintillation is wavelength-shifted and detected using a photomultiplier (PMT). (Thus these single P.E. pulses are called "afterpulses".) A typical PMT oscilloscope trace from our experiment described in this paper is shown in Fig. 1.

One distinct difference between α tracks and electron tracks is the ionization density. For example, a 5.5-MeV α particle deposits energy into superfluid liquid helium ($\rho = 0.145$ g/cm^3) at a rate of 2.0×10^4 eV/μm on average along its 0.27 mm long track[43], whereas for a 500 keV electron, the average energy deposition rate is 40 eV/μm [13]. With $W = 43$ eV, it follows that ionization events are separated by an average distance of ~ 2 nm and ~ 900 nm in α and electron tracks, respectively. With an average separation of 20 nm between the electron and its parent ion [14], ionization events in α tracks overlap with each other whereas ion-electron pairs are well separated in electron tracks. As we will discuss later, many of the differences in the characteristics between α-induced scintillation and electron-induced scintillation can be attributed to the difference in the ionization density.

In establishing the picture described above, a study of scintillation in the presence of an electric field played an important role. The effect of an application of an electric field on the LHe scintillation was first studied by Hereford and Moss [15]. In this study, the authors measured both the intensity of α-particle-induced scintillation and the ionization current extracted from the α tracks in the presence of an electric field (9 to 43 kV/cm) in the temperature range of 1.23 to 4.2 K. The scintillation signal was integrated over ~ 1 μs. They observed a decrease in the scintillation intensity and a corresponding increase in the ionization current with an increasing electric field. They concluded that recombination luminescence accounts for approximately 60% of the total scintillation intensity with zero electric field and that this component of the intensity is temperature independent.

We have extended their work and have studied the effect of an application of an electric field on both the prompt scintillation and afterpulses in the temperature range of 0.2 K to 1.1 K with an electric field up to ~ 45 kV/cm. We measured the time dependence of the scintillation signal up to 14 μs.

This work was motivated by the application of superfluid helium as a scintillator in the presence of an electric field, in particular, for the nEDM experiment [16, 17]. The nEDM experiment, currently being developed to be mounted at the Spallation Neutron Source at the Oak Ridge National Laboratory, will search for the neutron electric dipole moment using a method proposed by Golub and Lamoreaux [18].

II. EXPERIMENTAL APPARATUS AND PROCEDURE

A. Overview

The experiment was performed using a Leiden Cryogenics model CF-600 cryogen free dilution refrigerator [20], which had a measured cooling power of 1.8 mW at 0.2 K. A measurement cell, which housed the electrodes immersed in LHe, was mounted on the mixing chamber of the dilution refrigerator (DR). An ^{241}Am α source was electroplated on the ground electrode. α particles from the source induced scintillation light in the volume of LHe between the electrodes. The EUV scintillation light was converted to blue light by a wavelength shifter, then was guided through a light guide to the viewport at the bottom of the measurement cell and to a photomultiplier tube mounted outside the measurement cell in vacuum. A description of each component is given below.

B. Measurement cell, the electrodes, and the PMT

A schematic of the measurement cell and the PMT is shown in Fig. 2. The measurement cell was made of a stainless steel cross with 4-5/8" and 4-3/4" conflat flanges attached to its ends. The volume of the LHe inside the cell was approximately 600 ml. At the top of the cell was a heat exchanger made of stack of gold-coated copper plates, which provided cooling from the mixing chamber to the LHe inside the cell.

The electrodes were made of stainless steel. The ground electrode was 19.05 mm in diameter and 6.35 mm

in thickness, and had an edge rounded with a radius of 3.175 mm. The high voltage (HV) electrode was 19.05 mm in diameter and 12.7 mm in thickness, and had an edge rounded with a radius of 6.35 mm. The gap between the electrodes was approximately 4 mm.

The HV electrode was mounted on a commercially made HV vacuum feedthrough. The HV was supplied by Glassman Model EH30R3 power supply. A thin wall stainless steel tubing was used as the HV wire inside the cryostat to reduce the heat load. In order to reduce the effect of the ripple of the HV power supply on the PMT signal (the PMT picked up the noise induced by the ripple of the supply), a HV resistor ($R = 1$ GΩ or $R = 1$ MΩ) was inserted in series in the HV cable. The capacitance of the HV cable and this resistor formed a low pass filter to reduce the effect of the ripple to a sufficiently low level.

Approximately 300 Bq of ^{241}Am was electroplated on the ground electrode. The activity had a diameter of 6 mm. Since the range of 5.5 MeV α particles in superfluid liquid helium is only $\sim$ 0.3 mm, the ionization due to α particles occurred in a region very close to the surface of the ground electrode. The electric field at the location of the ionization was uniform to 5%. The size and shape of the electrodes were chosen as a compromise between field uniformity and the solid angle subtended by the TPB-coated acrylic surface at the ionization (see below).

The electrodes were enclosed in a sleeve made of G10. This was to prevent possible HV breakdowns due to the HV electrode seeing structures on the inner walls of the stainless steel measurement cell.

A sapphire viewport with a view diameter of 49.3 mm was mounted at the bottom of the measurement cell. An acrylic light guide with a diameter of 49.3 mm and a length of 30.5 mm was mounted between the viewport and the G10 sleeve. (The G10 sleeve had a hole on the side to allow the scintillation light to reach the light guide.) The top surface of the light guide was coated with polystyrene doped with tetraphenyl butadiene (TPB), which is known to have good EUV-visible conversion properties (see Ref. [21] and references therein). A Hamamatsu R7725 PMT, modified for cryogenic use with a Pt underlayer [22], was mounted underneath the viewport in vacuum.

Thus, a fraction of the α particle induced EUV light emitted from the region between the electrodes was converted to blue light at the surface of the light guide. The blue light was then guided towards the PMT through the light guide, transmitted through the sapphire viewport and then detected by the PMT. The fraction of the EUV light that reached the TPB coated surface of the light guide was about 5% (determined by the solid angle subtended by the coated surface of the light guide at the location of scintillation events).

The PMT was thermally anchored to the 3 K plate of the DR (which was cooled by a pulse-tube refrigerator) in order to reduce heat load, both radiative and conductive,

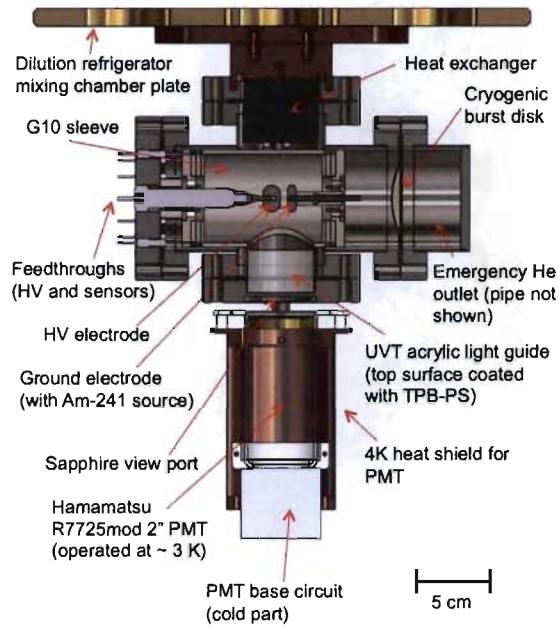

FIG. 2: Schematic of the apparatus

to the measurement cell. The base circuit adopted the split design described in Ref. [22] with some modifications. The resistor chain was heat-sunk on the 3 K plate. In order to reduce the heat load from the Joule heating of the resistor chain, a resistor value 10 times larger than the manufacturer recommended value was used. Because the event rate was low, this did not affect the performance of the PMT. The rest of the base circuit (mostly capacitors) was mounted at the back of the PMT. Previously, this PMT model had been demonstrated to function properly at temperatures down to $\sim$ 8 K [22]. The present work showed that it functions properly at $\sim$ 2.5 K.

There are two RuO_2 temperature sensors mounted on the G10 sleeve to monitor the temperature of the LHe inside the measurement cell. There are two LHe level sensors inside the measurement cell. They were each made of two concentric cylinders that form a capacitor. One was mounted in such way that it surrounded the heat exchanger and the other surrounded the light guide, monitoring the LHe level at the top and the bottom of the measurement cell. In addition there was a LHe pressure sensor monitoring the LHe pressure inside the measurement cell.

A silicon diode sensor was mounted on the PMT as well as the PMT heat shield to monitor the temperature

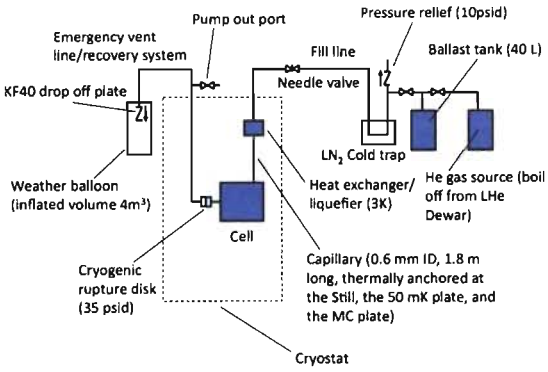

FIG. 3: Flow schematic

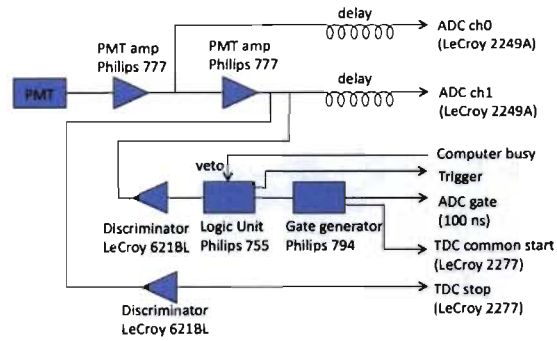

FIG. 4: Schematic diagram of the DAQ system

of the PMT and the heat shield.

C. Helium gas/liquid handling

A schematic of the helium gas/liquid flow in the system is shown in Fig. 3. In filling the system, clean helium gas (boiloff from a Dewar) was further cleaned by a LN_2 cold trap and then was introduced into the system. The helium was first condensed by a liquefier (a box filled with sintered metal) mounted at the 3 K plate, then flowed through a capillary tube with an ID of 0.6 mm and a length of 1.8 m which was thermally anchored at the still, the 50 mK plate, and at the mixing chamber plate to the measurement cell. The cell was filled with the DR running, which kept the cell temperature at ~ 0.9 K during the fill.

D. Data acquisition system

Data on the PMT signal were collected using a CAMAC and NIM based data acquisition system. The schematic of the DAQ system is shown in Fig. 4. The trigger was generated by a discriminator whose threshold was set to a level corresponding to a fraction of a photoelectron (P.E.), which allowed us to monitor the PMT gain using single P.E. events from the dark noise.

For each event, the size of the prompt signal was recorded using a Lecroy 2249A charge-sensitive analog-to-digital converter (ADC) with a 80 nm-long gate. The length of the gate was chosen to capture all of the prompt part of the signal (see Fig. 1). The PMT signal was split into two, one of which was amplified with a gain of ~ 7 before being fed to the ADC. The amplified signal was used to monitor the PMT gain using the single P.E. events from the dark noise. The unamplified signal was

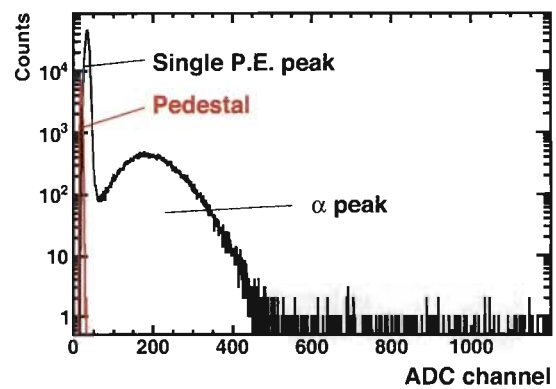

FIG. 5: Spectrum of the prompt signal

used to measure the size of the signal generated by α particles. Randomly generated pulses were mixed into the trigger in order to monitor the ADC pedestal. A typical low-gain ADC spectrum is shown in Fig. 5.

The timing of each afterpulse (see Fig. 1) with respect to the prompt pulse was recorded using a Lecroy 2277 multi-hit TDC. This TDC can record up to 16 hits within a 16 μs time window. Typical time spectra thus obtained are shown in Fig. 6 for two temperatures. Also a typical distribution of the number of afterpulses per event is shown in Fig. 7.

E. Experiment

The cell was filled with LHe following the procedure described in Sec. II C. Once the cell was filled and a desirable measurement cell temperature was reached, the prompt scintillation light intensity and the time spec-

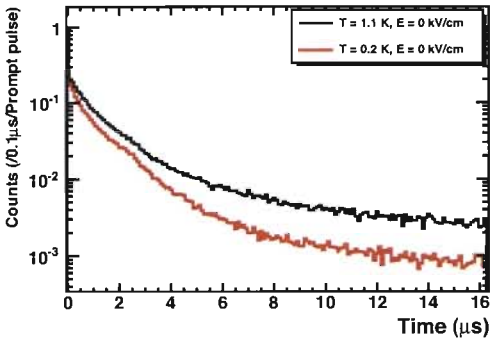

FIG. 6: Spectra of afterpulse timing with respect to the prompt pulse. The bump around 2.5 μs is due to afterpulses caused by helium contamination in the PMT.

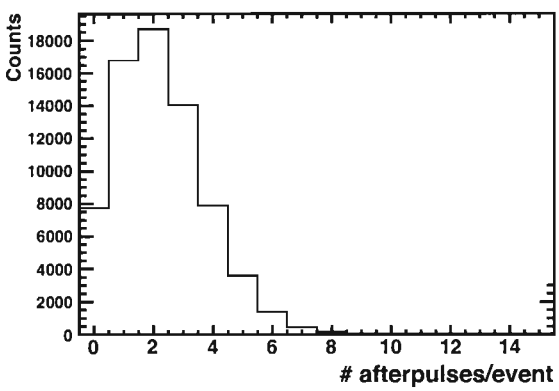

FIG. 7: Distribution of the number of afterpulses per event

trum of the afterpulses were measured as the function of the applied HV. When increasing or decreasing the HV, the PMT was kept turned off to protect the PMT from being exposed to bright flashes of light due to HV breakdowns, which occurred occasionally when changing the HV setting; we had found that exposing the PMT to flashes of light from HV breakdowns decreased the PMT gain and the change appeared to be permanent. The HV electrode was biased with a negative voltage. For each HV and temperature setting, data was acquired for approximately 5 minutes, which corresponds to $\sim 10^5$ scintillation events (each of such a continuous data taking period is called a "run").

Data were taken at nominal temperatures of 0.2 K, 0.3 K, 0.4 K, 1.0 K, and 1.1 K for electric fields up to approximately 45 kV/cm. The average temperatures and the 1-σ variations in the temperature for runs with the same nominal temperature were 220 ± 3 mK, 298 ± 3 mK, 397 ± 7 mK, 979 ± 12 mK, and 1084 ± 17 mK for nominal temperatures of 0.2 K, 0.3 K, 0.4 K, 1.0 K, and 1.1 K, respectively. In addition data were taken at temperatures up to 2 K with no HV applied.

As mentioned earlier, a HV resistor was inserted in the HV supply line to suppress noise due to the ripple on the HV. Most of the data were taken with a 1 GΩ resistor. We confirmed that the results did not change when a 1 MΩ resistor was used.

III. DATA ANALYSIS AND RESULTS

A. Analysis of the ADC data

Because we are interested in a change in the PMT signal due to the application of the electric field, it is important to remove all other possible sources that can cause a change in the PMT signal. In particular, the PMT gain shift needs to be properly accounted for in the analysis.

The analysis of the prompt pulse ADC spectra was performed following the following steps:

1. Determine the PMT gain from the location of the single P.E. peak in the high gain ADC spectra.
2. Determine the gain of the amplifier (Phillips 777) from the slope of the correlation between the high gain and low gain ADC spectra (see Fig. 8).
3. Properly normalize the low gain ADC spectra using the information obtained from the previous two steps
4. Fit to the low gain ADC to determine the location of the α peak, which gives the relative intensity of the prompt scintillation light.

In the last step, the spectrum was fit to the following model function (a Poisson distribution representing the distribution of the number of P.E.'s convoluted with a Gaussian distribution representing the PMT response):

$$f_{\mathrm{ADC}}(x) = N \sum_{k=1}^{\infty} \frac{\mu^k e^{-\mu}}{k!} \frac{1}{\sqrt{2\pi {\sigma_k}^2}} e^{-\frac{(x-Gk)^2}{{\sigma_k}^2}}, \quad (3)$$

where N is the overall normalization, x a variable corresponding to the ADC channel, μ the mean number of photoelectrons, and G the gain of the system (the ADC channel corresponding to one P.E.). σ_k is given by

$$\sigma_k = \sqrt{{\sigma_{\mathrm{PMT}}}^2 \cdot k + {\sigma_{\mathrm{ped}}}^2}, \quad (4)$$

where σ_{PMT} is the width of the response function of the PMT for single P.E. events and σ_{ped} is the width of the ADC pedestal. N, μ, and σ_{PMT} were varied in the fit. The factor k above was an adjustable parameter and was necessary to obtain a good fit.

Figure 9 shows the dependence of the prompt pulse intensity on the temperature with no electric field. Our data is qualitatively consistent with what was observed in Ref. [15]. Note that a direct comparison between our

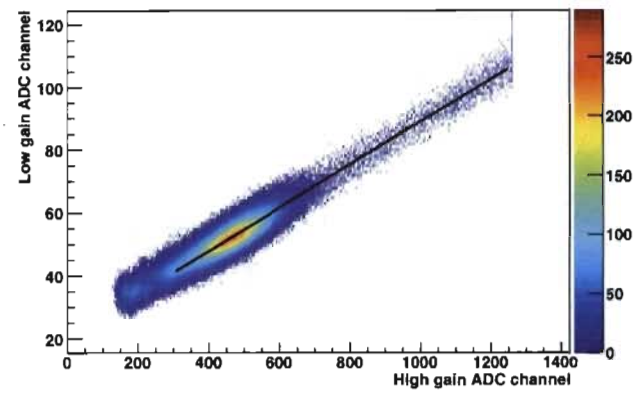

FIG. 8: The correlation between the high gain ADC and the low gain ADC data. The slope determines the gain of the PMT amplifier used for the high gain ADC.

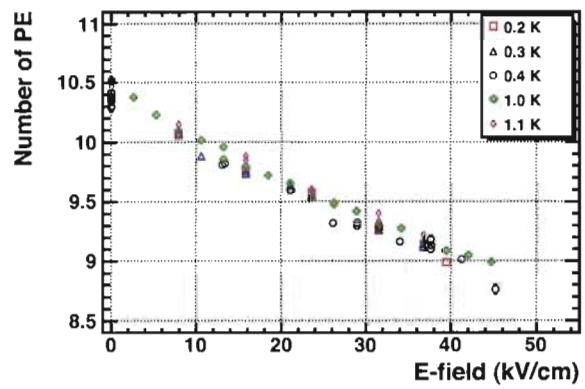

FIG. 10: The intensity of the prompt scintillation vs the electric field strength.

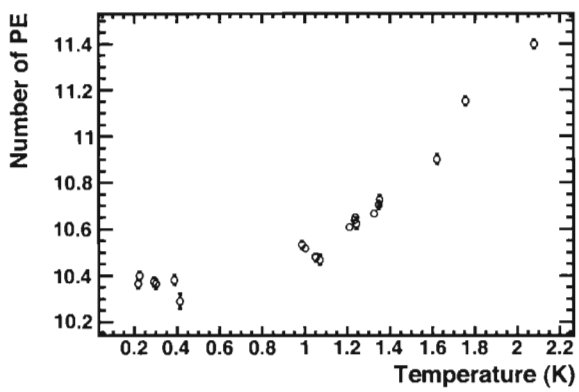

FIG. 9: The intensity of the prompt scintillation vs the temperature.

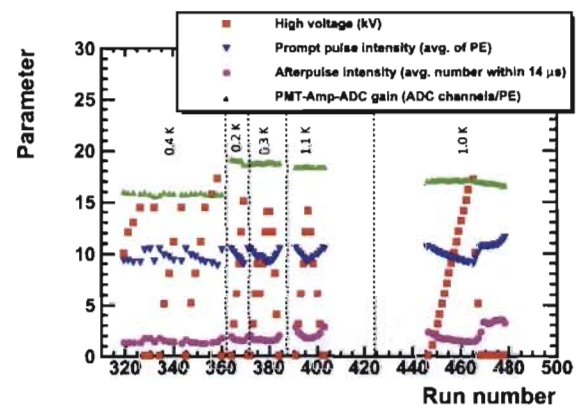

FIG. 11: Various parameters plotted against the run number

data and the data in Ref. [23] cannot be made because of the difference in the integration time for the prompt pulse.

Shown in Fig. 10 is the prompt pulse intensity plotted against the strength of the electric field for different temperatures. The prompt intensity decreases by about 15% with an electric field of 45 kV/cm. The effect of the electric field on the prompt intensity has little temperature dependence. Our results are qualitatively consistent with the results obtained by Ref. [15]. Note again that a direct comparison between our data and the data in Ref. [15] cannot be made because of the difference in the integration time for the prompt pulse.

Figure 11 plots the applied HV, the prompt pulse intensity, the afterpulse intensity (see Section III B), and the PMT gain as a function of the run number. The figure shows that, although the PMT gain changed throughout the course of the measurement, the change in the PMT gain was properly accounted for in the analysis. Note that the increase in the gain from the 0.4 K data to the 0.2 K data was due to the increased HV for the PMT bias.

B. Analysis of the TDC data

The mean number of afterpulses per event observed in the first 14 μs was determined by fitting a spectrum of the distribution of the number of afterpulses per event (Fig. 7) to a Poisson distribution. The mean number of afterpulses per event thus obtained is plotted against the temperature in Fig. 12. Our results, showing a reduction in the afterpulse intensity at lower temperatures, are consistent with Refs. [4] and [19]. [Note that, although Ref.[19] only shows a plot of the "pulse height" (the signal integrated for the first 1 μs) and the total intensity plotted against the temperature, the temperature depen-

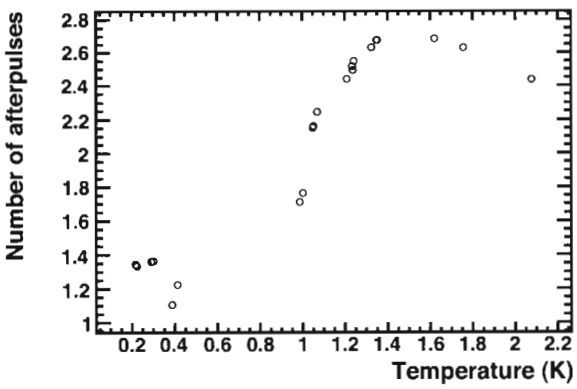

FIG. 12: Number of afterpulses per event plotted as a function of the temperature for zero electric field.

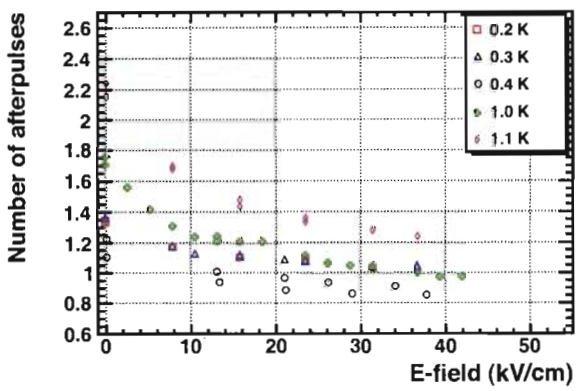

FIG. 13: Number of afterpulses per event plotted against the strength of the electric field.

dence of the afterpulse intensity can be inferred from the data.]

Figures 13 and 14 show the number of the afterpulses and the number of the afterpulses normalized to the prompt pulse intensity plotted against the strength of the electric field, respectively. We see from the figures that the afterpulse intensity decreases with an increasing electric field strength (Fig. 13) and that the afterpulse intensity is more strongly affected by the electric field than the prompt intensity (Fig. 14). Also, in contrast to the prompt scintillation, the effect of the electric field on the afterpulse intensity exhibits some temperature dependence.

IV. DISCUSSION

What we have observed from our data can be summarized as follows:

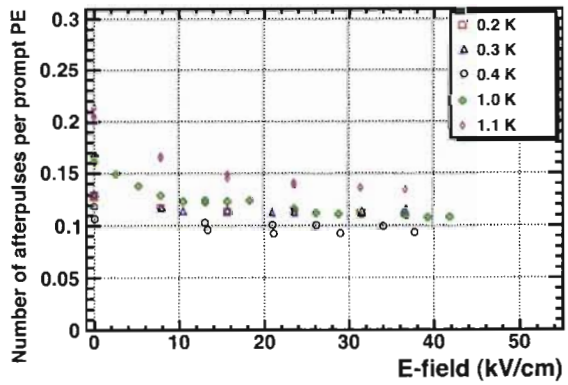

FIG. 14: Number of afterpulses per event normalized to the prompt pulse intensity plotted against the strength of the electric field.

1) The prompt intensity is reduced by 15% at ~ 45 kV/cm.
2) The reduction in the prompt scintillation yield is approximately linear in the strength of the electric field.
3) The effect of the electric field on the prompt pulse intensity has a very weak temperature dependence in the temperature range of 0.2 K to 1.1 K.
4) The electric field has a stronger effect on the intensity of the afterpulse than it has on the intensity of the prompt pulse.
5) The observed temperature dependence of the prompt and afterpulse intensities at zero electric field is in qualitative agreement with previous work.

Below we discuss the implication of these observations.

A. Effect of an electric field on the prompt pulse intensity

The prompt scintillation signal is the result of the radiative decay of singlet He* atoms in excited states and of He_2^* excimers also in singlet states. An α particle produces these atoms and excimers either by ionization followed by recombination or by promoting an atom directly to an excited state without ionization. The ratio of the number of direct excitations to ionizations has been predicted in helium to be [24] 0.45 : 1. (Although this calculation was performed with 100 keV electrons as the primary particle, the expectation is that it holds for α particles as well [25].) Among the atoms promoted directly to excited states the ratio of singlets to triplets was calculated to be 5:1. On the other hand, the ratio of singlets to triplets formed by recombination of ionized atoms is expected to be the statistical value of 1:3 for α particles (not the case when electrons are the primary ionizing particle [8]). Scintillation from atoms in

excited states that have previously not undergone ionization is not affected by an electric field whereas the number of those that been ionized is decreased in a field because of charge separation. Were there no other complicating factors the field-dependent fraction, x, of the prompt scintillation would be $x = 0.4$. However, a number of phenomena can influence this fraction, most likely increasing its value.

1) The prompt signal for α particles is substantially quenched [8] by the non radiative destruction of singlet excimers by the Penning process[Eq. (2)] but by the same mechanism it may be slightly enhanced with the destruction of triplet excimers and the subsequent recombination of the resulting ions into singlet states. Excited state singlet atoms may also non radiatively decay upon interaction with other species of excitations.

2) Singlet helium atoms in excited states with principal quantum number, n, of 3 or greater can autoionize by the Hornbeck-Molnar process [26]

$$\mathrm{He}^* + \mathrm{He} \rightarrow \mathrm{He}_2^+ + e^-, \tag{5}$$

since the binding energy of He_2^+ is$\sim$ 2 eV, which is greater than the energy to ionize a He(n$\geq$ 3) atom. Based on the oscillator strengths for the transitions between the ground state and the various excited states of helium [27] slightly more than one-third of the atoms promoted to excited states will have a principal quantum number of 3 or greater, the other two-thirds having n = 2. If all atoms with n$\geq$ 3 were to undergo autoionization, then the field-dependent fraction of the prompt scintillation would be increased to $x = 0.6$.

Various theoretical models have been developed that describe ion-electron recombination in an ionization track in fluid media: Jaffe's columnar theory of recombination [28, 29] describes the case in which a dense plasma of positive and negative ions is formed along the ionization tracks while Onsager's theory [31] describes the case where each ion-electron pair is spatially separated and recombination occurs between an electron and its parent ion (geminate recombination). For the highly ionizing track of an α particle in LHe the Jaffe model would appear the more applicable.

In the columnar theory, the rate of recombination is governed by the following equations:

$$\frac{\partial n_+}{\partial t} = -u_+ \boldsymbol{E} \cdot \nabla n_+ + D_+ \nabla^2 n_+ - \alpha n_- n_+, \tag{6}$$

$$\frac{\partial n_-}{\partial t} = -u_- \boldsymbol{E} \cdot \nabla n_- + D_- \nabla^2 n_- - \alpha n_+ n_-, \tag{7}$$

where n_+ and n_- are the densities of the snowballs and bubbles, u_+ and u_- are the mobilities, D_+ and D_- are the diffusion coefficients, and α is the recombination coefficient. What this model describes are clouds of negative and position ions being pulled away from each other by the electric field while at the same time recombining at a rate proportional to the product of their densities. Also, the clouds expand radially due to the diffusive motion of the charges.

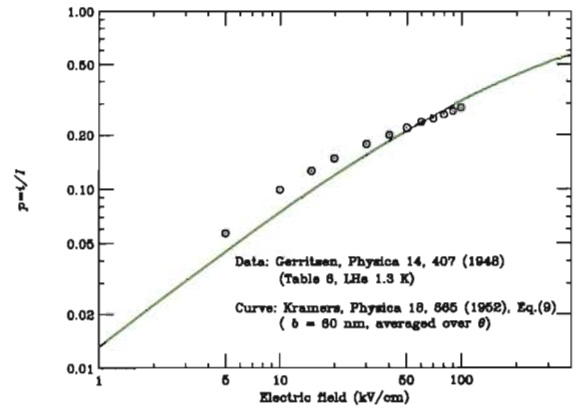

FIG. 15: The best fit of Kramers' theory to Gerritsen's data with $b = 60$ nm.

In looking for a solution to the these rate equations Jaffe assumed the diffusion terms were larger than those associated with recombination and hence, along with the field term, were the principal cause of the change in densities of the charges. This is a valid approach for ionization in gases. On the other hand, Kramers [29], in attempting to explain the electric field dependence of the ionization currents from α particles stopped in liquid helium measured by Gerritsen [30], pointed out that in a dense fluid the diffusivity of the ions is small and that recombination has a much larger influence on the time dependence of the charge density. Gerritsen's data for the electric field dependence of the ionization current can be fit approximately by the Kramers theory with a cylindrical Gaussian charge distribution having the same density and spatial distribution for n_+ and n_-

$$n_\pm(t=0) = \frac{n_0}{\pi b^2} e^{-r^2/b^2}, \tag{8}$$

where n_0 is the initial number of positive ion snowballs or electron bubbles per unit length along the track. The diffusion coefficient was assumed to be zero. The best fit of Kramers' theory to Gerritsen's data with the one adjustable parameter, $b = 60$ nm, is shown in Fig. 15.

Several comments regarding this result are relevant to understanding the scintillation and ionization currents of LHe.

1) The ionization current data contains contributions that are not included in the Jaffe-Kramers theory, which describes the ionization current due to charge carriers that escaped the initial recombination. However, at field strengths below that corresponding to the saturation current, charge carriers that initially recombine can contribute to the ionization current through processes such as Penning ionization [Eqs. (1) and (2)]. A crude estimate indicates that such contributions could be larger than 10%.

2) The Langevin relation between recombination coefficient and mobility is $\alpha = e(u_+ + u_-)/\epsilon_0$. In the approximation that the mobilities of the two species are the same, the electric field dependence of the current is independent of mobility, as it enters the recombination and field terms in the same manner. At the temperature within the track of approximately 2 K (see below), the mobilities of the positive and negative ions are approximately the same [32], having the value of $u_+ + u_- \sim 10^{-5}$ m^2/(V·s). Hence the recombination coefficient is $\alpha \approx 2 \times 10^{-13}$ m^3/s.

3) From the Einstein relation $D = kTu/e$, the diffusion coefficient is calculated to be $\sim 1.7 \times 10^{-5}$ m^2/s. Since the initial charge densities along the track are the order of 10^{22} m^{-3}, diffusion plays little role in affecting the density distribution at early times when recombination is dominant. At longer times when the concentrations have decreased substantially, diffusion can influence the charge separation.

4) The assumption that the positive ions and the electron bubbles initially have the same spatial distribution is unlikely to be correct. The ionization events from the α particle or from secondary electrons with energy sufficient to create further ionizations occur in a small cylinder about the track of less than 10 nm. He ions do not move appreciably in the time it takes for the electrons to thermalize and form a bubble. However, once the energy of secondary electrons drops below 20 eV, the first excited state of He, the only process by which they can lose energy is elastic scattering from helium atoms. Since the fraction of energy an electron loses in such a collision is very small, being dependent on the ratio of the mass of the electron to that of the atom, the order of 10^4 collisions are required to decrease an initial energy of 10 eV to below 0.1 eV thought to be necessary for bubble formation. From the cross section for elastic scattering, which varies from 3 to 6×10^{-16} cm^2 between 1 and 10 eV, and the liquid density, the mean free path is roughly $\ell \sim 1$ nm and the mean distance for diffusion, proportional to the square root of the number of scatters is the order of 100 nm [33]. But as Muñoz *et al.* [34] point out, if the initial positive and negative charge distributions are Gaussian with very different radii, then the radial field arising from the different charge distributions can be large, easily in the range of 100 to 1000 kV/cm for an α track in helium assuming 10 nm for the radius of the positive ions and 100 nm for the electrons. The two distinct distributions will therefore rapidly merge to form a more uniform distribution assumed in the Jaffe and Kramers theories. The positive ion snowballs having a mobility comparable to that of the electron bubble at the initial temperature of ~ 2 K along the track (see below), will expand outward and the electrons contract inward.

The measured electric field dependence of the prompt scintillation can be fit well using Kramers theory for a range of different Gaussian widths, b. The value of b depends on the choice of the fraction, x, of scintillation

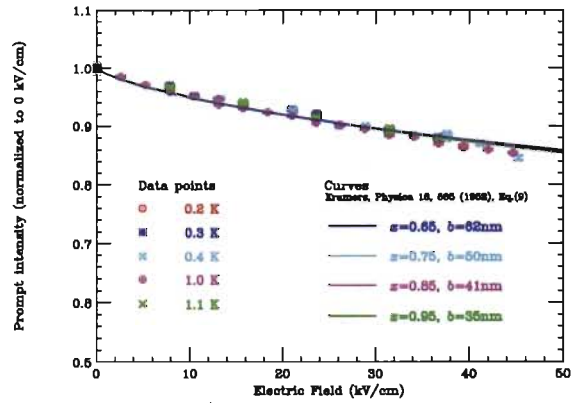

FIG. 16: Kramers theory fit to the measured electric field strength dependence of the prompt scintillation intensity

resulting from species created by ionization, which can be affected by the field (see Fig. 16). If x is taken to be 0.95 then the best fit is for $b = 35$ nm, while for $x = 0.65$, $b = 62$ nm.

A few comments about the relationship between ionization current and the effect of an electric field on the prompt scintillation intensity are appropriate. These two types of data reflect two different aspects of the same phenomenon, and as such it should be possible to construct a model that describe both data consistently. Indeed, such an analysis was performed by the authors of Ref. [15]. They concluded that approximately 60% of the observed scintillation intensity (with an integration time of ~ 1 μs) is due to recombination. However, such an attempt is complicated by a number of factors. 1) As mentioned earlier, the ionization current has a contribution from charge carriers that initially recombine. 2) There is uncertainty in the value of x. 3) Even with a short integration time (in our case ~ 80 ns), there is inevitably a contribution to the prompt signal from the delayed component, which has a different electric field dependence (see Sec IV.C). Because of these complications we have not attempted a unified analysis of our data and Gerritsen's ionization current data. However, we note that the choice of $x \approx 0.6$ and $b \approx 60$ ns is consistent both with our estimate of the fraction x and the best fit of Kramers' theory to Gerritsen's data.

As seen in Fig. 16, the effect of the electric field on the prompt intensity has little temperature dependence. This is attributed to three causes: 1) The effect of the electric field on recombination is nearly independent on the mobility of the ions as discussed earlier. 2) The initial temperature of the track is in the vicinity of 2 K, irrespective of the temperature of the bulk liquid (see below), resulting in the same mobility of ions in the track irrespective of the bulk liquid temperature. 3) The characteristic time of recombination $t_r = 1/(\alpha n_0)$, where n_0 is the initial ionization density, is faster than the time it takes the α track to thermalize with the bulk liquid, $t_{\rm therm} = b/c$,

where c is the sound velocity ($c \sim 230$ m/s). Indeed, with $b = 60$ nm, $n_0 \sim 4 \times 10^{22}/\mathrm{m}^3$, $t_r \sim 1 \times 10^{-10}$ s as compared to $t_{\mathrm{therm}} \sim 3 \times 10^{-10}$ s.

B. Temperature dependence of the prompt scintillation

The faction of energy of an α particle that is quickly down converted to excitations of the superfluid, phonons and rotons, is sufficient to heat a column of liquid a few tens of nanometers radius along the track to the vicinity of 2 K irrespective of how low the temperature of the bulk liquid [35]. Since the density of liquid helium changes by less that 0.5% below 2 K, the initial environment in which the electrons, ions, excimers and excited state atoms reside, on their creation, is independent of the temperature of the bulk liquid. Therefore, the temperature dependence of the prompt scintillation, illustrated in Fig. 9, must result from the manner in which those entities responsible for the scintillation are influenced by the expansion of the roton/phonon cloud (with velocity of $\sim 10^2$ m/s) taking place at times the order of 10^{-10} s. Below a temperature of 0.6 K the density of thermal excitations in the bulk liquid is so low that the hot columnar cloud expands into essentially a vacuum. But at higher temperatures the thermal excitations in the bulk become sufficiently dense to scatter and slow the radially expanding cloud.

As discussed below, the $1/t$ component of the afterpulse intensity also decreases with decreasing temperature. The temperature dependence of both the prompt and afterpulse signals is attributed to the more rapid decrease of the triplet excimer density due to expansion, leading to a reduced production of singlets via the Penning process.

Hereford and coworkers [19, 36], in modeling the temperature dependence of the scintillation they observed, argued that the increased diffusion at low temperatures results increased quenching, that is, the enhanced non radiative destruction of the singlet species. However, their argument was not informed by the fact that the roton and phonon densities in the vicinity of the track is essentially independent of the temperature of the bulk liquid.

C. Temperature and electric field dependence of the afterpulse scintillation

Following the work of McKinsey *et al.* [4] the time dependence of the afterpulse scintillation for times between 0.4 μs and 14 μs has been characterized using the function

$$f_{\mathrm{TDC}}(t) = Ae^{-t/\tau_s} + \frac{B}{t} + C. \tag{9}$$

τ_s, A, B, and C were varied in the fit. For convenience, we define N_A, N_B, and N_C to be the contributions to the

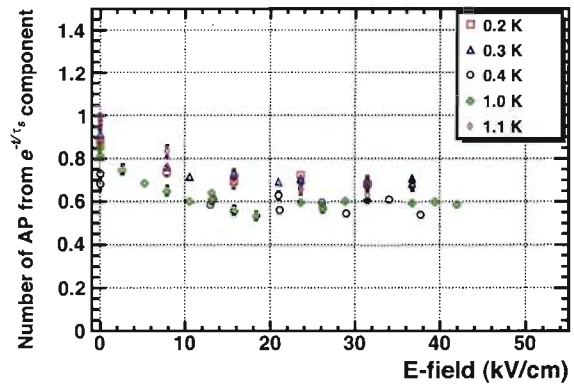

FIG. 17: N_A, the number of afterpulses from the exponential component (e^{-t/τ_s} *et al.*) in the afterpulse time spectrum plotted against the strength of the electric field.

number of afterpulses from the first, second, and third terms in Eq. 9, respectively, that is

$$N_A = \int Ae^{-t/\tau_s} dt, \tag{10}$$

$$N_B = \int \frac{B}{t} dt, \tag{11}$$

and

$$N_C = C \int dt. \tag{12}$$

N_A, N_B, and N_C are plotted as a function of the electric field for different temperatures in 17, 18, and 19 respectively. In Figs 17 and 18, the 1.0 K data points for electric fields between 10 kV/cm and 20 kV/cm seem to show a deviation from the apparent trend. We are not able to offer an explanation.

The value of τ_s that we obtained was ~ 1.3 μs, slightly shorter than the value quoted in Ref. [4]. Our results show that it is nearly independent of the temperature and the electric field.

Also in Fig. 20, N_B normalized to the prompt pulse intensity is plotted against the strength of the electric field for different temperatures.

At times longer than 10^{-7} s all singlet state excimers and excited atoms (except, perhaps, for the first excited state He(2^1S), which in vacuum has a lifetime of 19 ms [37]), will have long decayed. Any photons produced at a later time must result from triplet states.

1. *Component dependent exponentially on time*

McKinsey *et al.* [4] hypothesized that the afterpulse term dependent exponentially on time was the result of

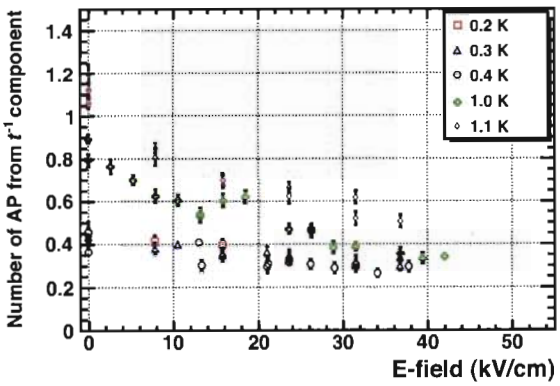

FIG. 18: N_B, the number of afterpulses from the t^{-1} component in the afterpulse time spectrum plotted against the strength of the electric field.

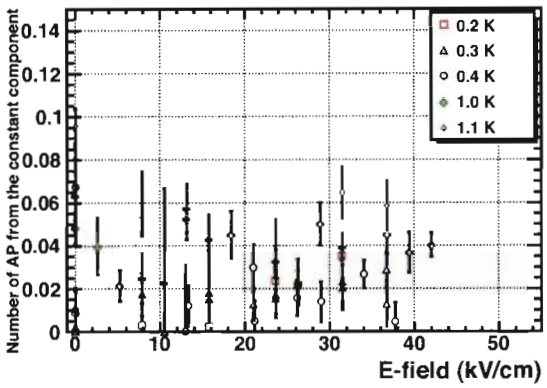

FIG. 19: N_C, the number of afterpulses from the constant component in the afterpulse time spectrum plotted against the strength of the electric field.

He(2^1S) atoms forming excimers in $A^1\Sigma_u^+$ states from which they radiatively decay to the dissociated ground state of the helium pair. Given that the lifetime of the triplet state He(2^3S) has been determined in the liquid to be 15 μs [38], this appears to be a reasonable hypothesis. Furthermore, there appears to be little or no temperature dependence to the exponentially time-dependent term, as expected for such a source. On the other hand, one would not expect that a signal arising from a neutral atom to exhibit a dependence on electric field as we have observed (see Fig. 19), unless it originated through recombination. Since the probability that ions form excimers prior to recombination is high, atomic He(2^1S) appears more likely to be produced by decay from a higher lying He(n^1P) state created de novo by electromagnetic excitation from the ground state than through a cascade from an atom formed by recombination. We are unable to offer an explanation of this exponentially time-dependent component of the afterpulse scintillation.

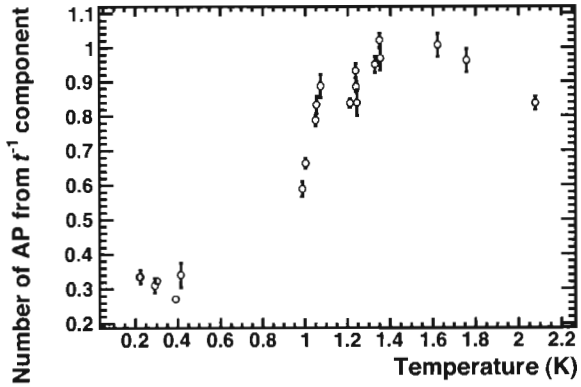

FIG. 20: The number of afterpulses the t^{-1} component in the afterpulse time spectrum normalized to the prompt pulse intensity plotted against the strength of the electric field..

2. *Component dependent inversely on time*

Keto *et al.*[40], using a beam of 160 keV electrons as the primary ionizing source, measured the long-time afterglow in the infrared spectra associated with a number of transitions between excited states of excimers and atoms to have a time dependence that varied as $1/t$. They ascribed this time dependence to the production of the excited states by the Penning ionization of triplet excimers, since the bimolecular process,

$$\frac{dn}{dt} = -\gamma n^2 \tag{13}$$

results in n proportional to $1/t$ for $\gamma t > 1$.

The problem of describing the time dependence of the afterpulse scintillation from an α particle differs from that in the work of Keto *et al.* [40] since in one case the density of excimers is uniform whereas in the other the excimer cloud is expanding about the α track.

King and Voltz [39] developed a theoretical model of afterpulses that includes the spatial evolution of the excimer density with time. The description involves the kinetics of the diffusion of the triplets at times well after the prompt scintillation has decayed. If the triplets maintain a Gaussian distribution as they expand by diffusion, then at long times the afterpulsing decreases approximately inversely with time. McKinsey *et al.* [4] cited this model by way of explaining the origin of the $1/t$ component of the afterpulses. At shorter times the King model predicts a time variation that is considerably faster the $1/t$, but it does not provide an explanation of the exponential dependence on time, as experimentally observed.

The amplitude of the $1/t$ afterpulse component exhibits interesting temperature and electric field dependences. Firstly, the number of afterpulses varies much more with temperature than the number of photons in the prompt scintillation. Secondly, the number of afterpulses decreases more rapidly with field than the prompt signal.

As with the slight variation of the prompt signal with temperature below 1 K, the rapid variation of the $1/t$ afterpulse component with temperature can be understood qualitatively as being the result of the change in propagation to the triplet excimers away from the α track. While the temperature within the core of the track is not sensitive to the ambient temperature of the liquid, the thermal excitations in the surrounding liquid can affect the rate at which the excimers expand away from the track. At high temperatures, the excimers diffuse slowly because of scattering from phonons and rotons, while at low temperatures the excimers propagate ballistically into the cold liquid. The excimer density drops much more rapidly a low temperatures and as a consequence the rate of generation of singlet species by the Penning process is strongly temperature dependent.

As for the electric field dependence of the $1/t$ component of the afterpulse scintillation, the initial production of triplet excimers is suppressed due to the electric field in the same manner as the production of singlet excimers that are suppressed. In addition, the electric field dependence of the $1/t$ component of the afterpulse scintillation, is related with the fact that the Penning bimolecular process creates a positive ion and an electron in isolation of other ionizing events, and as such the recombination is geminate.

Tachiya and coworkers [41] have pointed out that the Onsager theory of geminate recombination in which the charges move diffusively, is not valid when the mean free paths are comparable to other relevant dimensions. Tachiya considered this dimension to be the Onsager radius. $r_c = e^2/(4\pi\epsilon_0\epsilon kT)$, which for liquid helium at 1 K is 1.7×10^{-5} m. In our case the relevant dimension is the initial separation of the charges, which is expected to be less than 100 nm.

If recombination is occurring where the density of thermal excitations is comparable to a temperature of 0.6 K or below, the mean free paths of positive ion snowballs and electron bubbles are both in excess of 1000 nm, and their motion can be considered ballistic. Above 1 K, however, the density of thermal excitations is sufficiently large that the snowballs and bubbles can be treated as moving in a viscous medium. In the event diffusion is small, the charge move along field lines, and whether two charges recombine or not is dependent only on the magnitude and direction their initial separation with respect to an applied field. If $\boldsymbol{r}_0$ the initial separation and θ_0 is the angle between $\boldsymbol{r}_0$ and the applied field $\boldsymbol{E}$, the charges will recombine if

$$E < \frac{e}{4\pi\epsilon_0 r_0^2}(1 + \tan^2(\theta_0/2)) \ . \tag{14}$$

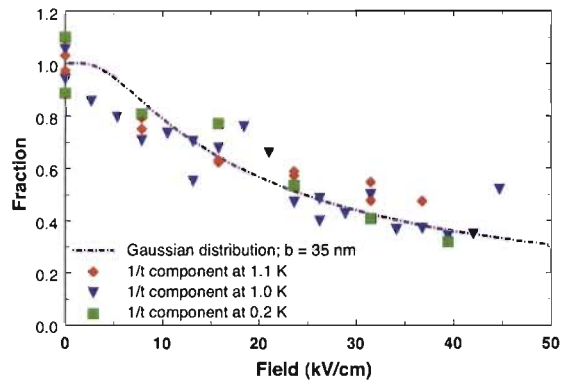

FIG. 21: A plot of the field dependence of the $1/t$ component at 1.0 K and at 1.1 K along with a curve calculated using Que's expansion and a Gaussian distribution with a width of 35 nm to describe the initial separation

For a distribution of electron/ion separations, $D(r)$, independent of orientation, the fraction of charges that will recombine is

$$1 - \int_{(\frac{e}{4\pi\epsilon_0 E})^{1/2}}^{\infty} D(r)r^2 dr(1 - \frac{e}{4\pi\epsilon_0 E r^2}) / \int_0^{\infty} D(r)r^2 dr. \tag{15}$$

Que and Rowlands[42] have obtained an expression for Onsager geminate recombination in the form of a power series expansion in electric field. For charges with a Gaussian distribution in helium at 1 K the results obtained using their series expansion differ from those of Eq. (15) only at low fields where the influence of diffusion is greatest.

A plot of the field dependence of the $1/t$ component at 1.0 K and at 1.1 K is illustrated in Fig. 21 along with a curve calculated using Que's expansion and a Gaussian distribution with a width of 35 nm to describe the initial separation. The dependence on the electric field through the initial production of the triplet excimers is removed in the plot, using the prompt scintillation data and assuming $x = 0.6$. As noted earlier, electrons from Penning process (Eqs. (1) and (2)) have a maximum energy of $\sim$ 10 eV. A Gaussian distribution of 35 nm is certainly not outside the range electrons of $\sim$ 10 eV are expected to travel before forming localized states.

We have not attempted to provide an analysis of the field dependence of the afterpulse signal at temperatures below 0.6 K where the motion of the charges is ballistic. Furthermore, the charges can acquire a velocity sufficient to create vortices in this regime.

3. *Component independent of time*

The constant component of the afterpulses, independent of time, is most naturally associated with triplet excimers whose density is constant and are uniformly distributed throughout the volume of the cell, the rate of destruction being balanced by the production from the 300 Bq α source. Destruction occurs in part by the spontaneous radiative decay of triplet excimers to the dissociated ground state and in part by the Penning process.

The most notable features of the data seen in Fig. 19 are the apparent weak field dependence of this afterpulse component at 1 K and the substantial decrease in intensity as the temperature is lower from 1 K to 0.4 K. These two properties are naturally explained by the scintillation being principally due to the spontaneous radiative decay of the excimers, the $a^3\Sigma_u^+$ state having a lifetime of 13 s in the bulk[11]. While the electric field is not expected to affect this process, it does lead to a decreased recombination and density of triplets with increasing field. Below about 0.6 K the mean free path of the excimers becomes long, comparable to the dimensions of the helium cell, so that non radiative destruction of the excimers on solid surfaces decreases the photon yield at low temperatures.

One observation remains unexplained. Hereford and coworkers[19, 36] noted that the total scintillation below 0.5 K depended on the geometry of their cell, the smaller cell having somewhat greater light output. The scintillation intensity decreased with decreasing temperature to a minimum at 0.4 K and then increased on going from 0.4 K to 0.2 K. We have observed similar behavior of the time-independent component of the afterpulse signal at low temperatures (see Fig. 12).

V. CONCLUSION

The prompt scintillation signal from α particles stopped in helium exhibits a 15% reduction in an electric field of 45 keV/cm. This field dependence is consistent with the current versus field measurements of Gerritsen[30] and Kramers' analysis of columnar recombination. We conclude using Kramers' theory that 40% of the scintillation results from species formed from atoms originally promoted to excited states by the α particle and 60% from excimers created by ionization and subsequent recombination, with the electrons initially having a cylindrical Gaussian distribution about the α track of 60 nm.

The delayed scintillation signal, the time dependence of which is decomposed in the manner suggested by McKinsey *et al.*[4], exhibits stronger field and temperature dependences than does the prompt scintillation. The stronger field dependence is the consequence of the fact that the slow component of afterpulses are from triplet excimers undergoing the Penning ionization process followed by recombination forming singlet excimers.As such,it receives the effect of the electric field twice, once at the initial recombination producing triplet excimers, and once at the recombination following the Penning process. The temperature dependence involves the diffusion of the excimers away from the hat α track into the surrounding bulk liquid.

VI. ACKNOWLEDGMENTS

The authors are grateful for the help and advice provided by the following individuals at various stages of this work: E. Bond, M. Fanning, S. Currie, D. G. Haase, G. Frossati, R. Golub, E. Korobkina, C. Nelson, J. Self, B. Lozoski, T. Rinckel, D. Baxter, W. M. Snow, and A. Edwards. This work was supported by the US Department of Energy, the National Science Foundation, and the DOE MIE #71RE..

[1] E. H. Thorndike and W. J. Shlaer, Rev. Sci. Instrum, **30**, 838 (1959).
[2] H. Fleishman, H. Einbinder, and C. S. Wu, Rev. Sci. Instrum. **32**, 1173 (1961).
[3] S. R. Bandler *et al.*, Nucl. Instum. Methods. A **370**, 138 (1996).
[4] D. N. McKinsey *et al.*, Phys. Rev. A **67**, 062716 (2003).
[5] P. B. Dunscombe, in *Liquid Scintillation Counting, Vol. 1*, edited by A. Dyer (Heyden and Son Ltd., London, 1971), Chapter 4, pp.37-42.
[6] N. Schwentner, E.-E. Koch, and J. Jortner *Electronic Excitations in Condensed Rare Gases* in Springer Tracks in Modern Physics **107**, (Springer-Verlag, Berlin, Heidelberg, New York, Tokyo, 1985), Section 6.6.2, pp.138-147.
[7] D. N. McKinsey, Ph.D. thesis, Harvard University, 2002.
[8] J. S. Adams, Ph.D. thesis, Brown University, 2001.
[9] W. Guo, D. Jin, G. M. Seidel, and H. J. Maris, Phys. Rev. B **79**, 054515 (2009).
[10] W. P. Jesse and J. Sadauskis, Phys. Rev. **97**, 1668 (1955). N. Ishida, J. Kikuchi and T. Doke, Jpn. J. Appl. Phys. **31**, 1465 (1992).
[11] D. N. McKinsey, *et al.*, Phys. Rev. A **59**, 200 (1999).
[12] A. V. Konovalov and G. V. Shlyapnikov, Soviet Physics JETP **73**, 286 (1991).
[13] M. J. Berger, J. S. Coursey, M. A. Zucker, and J. Chang, *ESTAR, PSTAR, and ASTAR: Computer Program for Calculating Stopping-Power and Range Tables for Electrons, Protms and Helium Ions*, National Institute Of Standards and Technology, Gaithersburg, MD (2005), `http://physics.nist.gov/Star` [Originally published

as: M. J. Berger, NISTIR 4999, National Institute of Standards and Technology, Gaithersburg MD (1993)].
[14] A. G. Tenner, Nucl. Instrum. and Methods **22**, 1 (1963).
[15] F. L. Hereford and F. E. Moss, Phys. Rev. **141**, 204 (1966).
[16] The nEDM experiment (M. D. Cooper and B. W. Filippone, spokespersons), `http:p25ext.lanl.gov/edm/edm.html`.
[17] T. M. Ito, J. Phys. Conf. Ser. **69**, 012037 (2007).
[18] R. Golub and S. K. Lamoreaux, Phys. Rep. **237**, 1 (1994).
[19] H. A. Roberts and F. L. Hereford, Phys. Rev. A **7**, 284 (1973).
[20] Leiden Cryogenics, B.V. `http://www.leidencryogenics.com`
[21] D. N. McKinsey *et al.*, Nucl. Instrum. Methods Phys. B **132**, 351 (1997).
[22] H.-O. Meyer, Nucl. Intrum. and Methods Phys. Res. Sect. A **621**, 437 (2010).
[23] M. R. Fischbach, H. A. Roberts and F. L. Hereford, Phys. Rev. Lett. **23**, 462 (1969).
[24] S. Sato, K. Okazaki and S. Ohno, Bull. Chem. Soc. Jpn. **47**, 2174 (1974).
[25] S. Sato, K.Kowari and K. Okazaki, Bull. Chem. Soc. Jpn. **49**, 933 (1976).
[26] J. A. Hornbeck and J. P. Molnar, Phys. Rev. **84**, 621 (1951).
[27] J. Berkowitz, J. Phys. B, **30**, 81 (1997).
[28] G. Jaffe, Ann. Phys. **42**, 303 (1913).
[29] H. A. Kramers, Physica **18**, 665 (1952).
[30] A. N. Gerritsen, Physica **14** 407 (1948).
[31] L. Onsager, Phys. Rev. **54**, 554 (1938).
[32] R. J. Donnelly and C. F. Berenghi, J. Phys. Chem. Ref. Data **27**, 1220 (1998).
[33] A. V. Benderskii, R. Zadoyan, N. Schwentner, and V. A. Apkarian, J. Chem. Phys. **110**, 1542 (1999).
[34] R. C. Muñoz, J. B. Cumming and R. A. Holroyd, J. Chem. Phys. **85**, 1104 (1986).
[35] S. R. Bandler, *et al.* Phys. Rev. Lett. **74**, 3169 (1995).
[36] H. A. Roberts, W. D. Lee and H. L. Hereford, Phys. Rev. A **4**, 2380 (1971).
[37] R. S. Van Dyck, C.E. Johnson and H. A. Shugart, Phys. Rev. A **4**, 1327 (1971).
[38] J. W. Keto, F. J. Soley, M. Stockton and W. A. Fitzsimmonns, Phys. Rev. A **10**, 872 (1974).
[39] T. A. King and R. Voltz, Proc. Roy. Soc. Lond. A **289**, 424 (1966).
[40] J. W. Keto, F. J. Soley, M. Stockton and W. A. Fitzsimmonns, Phys. Rev. A **10**, 887 (1974).
[41] H. Sano and M. Tachiya, J. Chem. Phys. **71**, 1277 (1979). M. Tachiya, ibid. **89**, 6929 (1988). M. Tachiya and W. F. Schmidt, ibid. **90**, 2741 (1989).
[42] W. Que and J. A. Rowlands, Phys. Rev. B **51**, 10500 (1995).
[43] The maximum energy deposition rate is 3.9×10^4 eV/μm and occurs when the remaining kinetic energy is 0.65 MeV.